Petroleum Science 21 (2024) 2663–2676

Contents lists available at ScienceDirect

Petroleum Science

journal homepage: www.keaipublishing.com/en/journals/petroleum-science

Original Paper

Optimized parameters of downhole all-metal PDM based on genetic algorithm

Jia-Xing Lu [a, b], Ling-Rong Kong [a, b, *], Yu Wang [a, b, **], Chao Feng [a, b], Yu-Lin Gao [a, b]

[a] China University of Geosciences (Beijing), Beijing, 100083, China
[b] Key Laboratory on Deep Geo-Drilling Technology of Ministry of Natural Resources, Beijing, 100083, China

ARTICLE INFO

Article history:
Received 25 May 2023
Received in revised form
27 March 2024
Accepted 27 March 2024
Available online 29 March 2024

Edited by Jia-Jia Fei

Keywords:
Positive displacement motor
Genetic algorithm
Profile optimization
Matlab programming
Overflow area

ABSTRACT

Currently, deep drilling operates under extreme conditions of high temperature and high pressure, demanding more from subterranean power motors. The all-metal positive displacement motor, known for its robust performance, is a critical choice for such drilling. The dimensions of the PDM are crucial for its performance output. To enhance this, optimization of the motor's profile using a genetic algorithm has been undertaken. The design process begins with the computation of the initial stator and rotor curves based on the equations for a screw cycloid. These curves are then refined using the least squares method for a precise fit. Following this, the PDM's mathematical model is optimized, and motor friction is assessed. The genetic algorithm process involves encoding variations and managing crossovers to optimize objective functions, including the isometric radius coefficient, eccentricity distance parameter, overflow area, and maximum slip speed. This optimization yields the ideal profile parameters that enhance the motor's output. Comparative analyses of the initial and optimized output characteristics were conducted, focusing on the effects of the isometric radius coefficient and overflow area on the motor's performance. Results indicate that the optimized motor's overflow area increased by 6.9%, while its rotational speed reduced by 6.58%. The torque, as tested by Infocus, saw substantial improvements of 38.8%. This optimization provides a theoretical foundation for improving the output characteristics of all-metal PDMs and supports the ongoing development and research of PDM technology.

1. Introduction

With the increasing drilling depths in deep and ultra-deep wells, the temperature conditions at the bottom of the borehole have become highly demanding. The positive displacement motor (PDM) utilizes an all-metal stator and rotor, whereby the performance output greatly relies on the precise gap fit and the distinct end profiles (Li et al., 2017; Tschirky, 1978). Consequently, the structural parameters of the all-metal PDM play a critical role in determining its performance output. To address this, the genetic algorithm, known for its accuracy in solving optimal solutions for multiple objective function combinations, was employed to optimize the PDM. By utilizing the genetic algorithm, the optimal performance parameters for the motor were successfully obtained.

The all-metal PDM was developed from the conventional PDM, also known as the all-metal fixed displacement motor, which is a volumetric bottom-hole power motor. In the early days, the PDM was manufactured by the United States of America as the first downhole drilling motor, named the Dina motor (Lu et al., 2023). In 1930, Rene Moineau in France designed the single screw based on the research of Archimedes' spiral, where the screw rotor is a single-wire spiral surface and the stator is a bushing barrel embedded with a double-wire spiral surface. Subsequently, he co-founded the first single screw manufacturing company with Robert Bienaime (Wang et al., 2022). In 1962, the development of a bore bottom motor with practical applications began to be manufactured into products. With the continuous improvement of PDM manufacturing technology, the optimization of the performance of the PDM has received more and more attention from research scholars, especially the study of the end-face line of the PDM. In 1966, the Perm Branch of the Soviet Drilling Technology Research

* Corresponding author. China University of Geosciences (Beijing), Beijing, 100083, China.
** Corresponding author. China University of Geosciences (Beijing), Beijing, 100083, China.
E-mail addresses: lrkong@email.cugb.edu.cn (L.-R. Kong), wangyu203@cugb.edu.cn (Y. Wang).

https://doi.org/10.1016/j.petsci.2024.03.022

Institute began to develop a special model of multi-head PDM, as opposed to the Dina screw's high speed, low torque, and poor adaptability with the tooth wheel drill bit and other shortcomings. This excellent improvement contributed to the further development of the screw, which has the characteristics of high output at low speed and high torque (Lea et al., 1988; Marius, 2018).

In the mid to late 20th century, as the screw line continued to be studied in depth, the high speed and low torque characteristics of the single-headed screw became increasingly unsuitable for directional good applications. The research scholars began to study the development of multi-headed screw lines, including Schlumberger, Baker, Christensen, and many other companies drilling equipment through a series of development of their own multi-headed screw products (El-Abd et al., 2020; Wang et al., 2021). In 1978, the Institute of Petroleum Exploration and Development Science research project "LZ6 1/2 screw development", the first 3-head screw, after years of research and development, screw manufacturing and application formed the specifications and series gradually dominate the market. In the 1990s, research scholars from the conventional screw in the case of clearance can also work inspired by the all-metal screw gradually known. So, the PDM can no longer use the inclusion of a rubber bushing stator, the stator and rotor clearance fit can also work. Canada has developed an all-metal PDM with a tungsten carbide and cobalt-bonded coating on the stator surface (Tschirky, 1978). The screw developed by G-PEX USA is made of synthetic material, and the stator is made of synthetic material with higher wear resistance than steel, to which friction-reducing reagents are added (Cao et al., 2022; Liang et al., 2023). However, the lifting performance and service life of all-metal PDM under clearance fit is significantly lower than that of conventional rubber screws, while the high temperature and corrosion resistance is significantly better than that of conventional rubber screws. Therefore, the optimization of PDM performance, focusing on the optimization of stator and rotor line shape, due to the specificity and complexity of the PDM line shape has not been able to achieve greater development, and genetic algorithm from the mathematical model theory (Nguyen et al., 2014; Whitley, 1994). The data points of the PDM stator and rotor curves are cross-sectionally, variably fitted and optimized. The structure is further optimized to improve the force of PDM, improve the lifting capacity and reduce the wear, and enhance the usability.

In 1960, the screw research scholars first conducted experimental test work on the optimal design of screw line profiles in terms of screw profile development. These determine the geometric structural characteristics of the screw, according to the working principle of the screw. Through the experimental testing of the rotational motion characteristics and laws of the screw, a model of the mechanical relationship between the lift in the work of the screw and the calculation formula was established. Secondly, the force deformation, the linear meshing change, and the effect on the sealing cavity of the screw stator rubber are studied (Nguyen et al., 2021; Rong et al., 2021). In 1993, Samuel and Saveth (2006) proposed to optimize the displacement and overflow area of the screw, and the improvement of the finishing performance was not satisfactory. Subsequently, Gaymard et al. (1988) optimized the stator and rotor engagement of the screw and improved the design by means of the rubber structure and dimensional parameters of the screw stator (Guo and Tang, 2003; Lehman, 2004). The mechanical analysis of the screw motor life and other aspects of the screw performance optimization at a later stage were improved by the majority of scholars. Wan (1993) proposed a single-screw hydraulic machinery optimization design for structural parameter optimization. They also established a mathematical optimization program through the computer (Marius, 2018; Samuel and Saveth, 2006). Firstly, according to the displacement of screw, the inertia caused by eccentricity, and the wear between the stator and rotor, the structural parameters of the screw are optimized. The matching of stator and rotor and the geometric characteristics of different screw lines are compared and analyzed by computer. Secondly, through the calculation and analysis of several linear shapes, it is concluded that the short internal oscillation of the screw is more suitable for the working characteristics of the screw.

In the aspect of genetic algorithm optimization, with the development of computer algorithm, more and more engineering problems apply this algorithm to optimize, especially the performance of data processing is very superior. In the 1990s, the genetic algorithm created by Professor Holland of the University of Michigan was suitable for adaptive probabilistic optimization of complex system optimization. It is also applied to the spiral optimization of the problem solution set as the population, that is, the optimal solution of the spiral equation is the population. A coded composition of individuals with characteristics (Chaturvedi et al., 2023; Whitley, 1994). Then, the initial generation of populations is generated and the best approximate solution is generated by iterative evolution according to the law of merit retention. In each iteration of the population, the better value is selected based on the size of the fitness of the individuals in the population. A new population of better solutions is generated using the combined crossover and variation approach in the genetic method, making the solutions in the population more suitable for the optimization objective of the problem. The traditional PDM design method mainly relies on empirical methods such as the experimental method and empirical formula derivation, which have the problems of low design efficiency and high cost (Rong et al., 2021; Zhang et al., 2022). Further, with the increasing development of computational methods and support tools in modern engineering design, computer simulation optimization of PDM has been considered for further design optimization.

However, the complexity and variability of the optimization model of the PDM make the modeling of the optimization problem very important. For the PDM optimization problem, we can classify it into single-objective and multi-objective optimization problems according to the expressions of its objective function. Genetic algorithm optimization PDM key steps: (1) The initial population, screw initial population and each iteration of the search process, the number of individuals included with the number of changes in the screw optimization calculation efficiency, and results have some relevance. (2) The objective function, the final optimization of the screw to achieve the goal of the conditional adaptation, is mainly used to assess the solution indicators of the function, the stronger the adaptation, the better the target solution, and its design have a direct correlation to the speed of convergence of the algorithm and the optimal solution. (3) Genetic operation process, the core operations of the genetic algorithm include selection, crossover, and mutation. The selection operator is used to select individuals with good fitness, usually by roulette-ranked selection. The crossover operator is used to cross two parental genes to produce new offspring. The mutation operator refers to random mutations in chromosomal genes to increase the diversity of the population. For the operation process of the genetic algorithm, we

need to carry out continuous practice and improvement to obtain a better optimization effect. (4) The evaluation of optimization results, the evaluation of optimization results mainly includes two aspects, one is the evaluation of the feasibility of the program, that is, whether the optimized PDM meets the design requirements, including performance indicators and parameters requirements (Baskal, 2014; Beauquin et al., 2005). The general form of the mathematical model for its optimal design is as follow Eq. (1).

$$\begin{cases} \min f(x) = f(x_1, x_2, \ldots, x_n) \\ \text{s.t. } g(x) \le 0 \\ h(x) = 0 \\ Ax \le b \\ Aeqx = beq \\ C(x) \le 0 \\ Ceq(x) = 0 \\ lb \le x \le ub \end{cases} \tag{1}$$

where $f(x)$ is the objective function in the genetic algorithm. s.t. is the abbreviation of "subject to". $g(x)$ and $h(x)$ are both constraints in the genetic algorithm. $Ax \le b$ is a linear inequality constraint. $Aeqx = beq$ is a linear equation constraint. $C(x) \le 0$ is a nonlinear inequality constraint. $Ceq(x) = 0$ is a nonlinear equation constraint. $lb \le x \le ub$ is a boundary constraint.

The linear optimization of the PDM to improve the output performance of the motor is mainly the simulation calculation, simulation analysis, and numerical simulation at present. The method of solving the probability distribution is seldom used, and there is an incomplete analysis. Therefore, in order to make the design results conform to the principle of a practical working environment, the genetic algorithm optimization screw is selected as a new method to solve the problem. It does not need an accurate mathematical model, but also has good global search ability, and can solve the complex multi-objective optimization problem well. Compared with other numerical simulation methods, the genetic algorithm has the following three advantages: (1) Based on PDM theoretical mathematical model, it can carry out in-depth optimization from linear formula theoretical parameters. (2) With the multi-objective genetic algorithm, multiple parameters can be optimized. (3) Genetic algorithm iteratively optimizes the objective function for many times, crosses and mutates the generated linear parameters, and selects the best solution with multiple parameters to optimize the target. Therefore, the genetic algorithm optimizes the principle as shown in Fig. 1.

It can be seen from Fig. 1, 'Front' is used to represent data ordering, and 'Gen' is used to represent the number of optimization iterations in a multi-objective genetic algorithm. In addition, in the all-metal PDM finite element simulation, Cao et al. (2022) used finite element analysis to conduct a more detailed analysis of the friction and wear of the all-metal progressive cavity pump. It has made an outstanding contribution to the research on the geometry friction and wear of all-metal progressive cavity pumps. In this paper, the genetic algorithm is a combination optimization method, which is based on the basic theory of the all-metal progressive cavity motor, to optimize the parameters and profile of the motor, and then get the best parameter combination of output torque.

In this paper, firstly, based on the geometry principle of the PDM cycloid generation profile, the motor end face profile is fitted accurately by the least squares method. Next, a mathematical model of the screw output characteristics is calculated numerically, and a genetic algorithm is introduced to optimize the parameters of the PDM profile. Finally, the motor parameters were optimized by the motor based on the genetic algorithm. The influence of the change of the isometric radius coefficient on the overflow area of the motor, the initial contour and the output characteristics after optimization are analyzed. It was obtained that the overflow area of the optimized motor increased by 6.9%, the rotational speed decreased by 6.58%, and the output power torque increased by 12.21%, while the output characteristics of the motor developed by Infocus. The comparison of the output characteristics of the PDM developed by Infocus shows 27.2% reduction in speed and 38.8% increase in torque, which provides a reference for the development of the profile and a theoretical basis for optimizing the output characteristics of the all-metal PDM.

2. Mathematical model

2.1. Curved design

The design of the line shape affects the value of the motor's over-flow area, curvature, and volume. So, this section describes the design of the line shape for all-metal PDM. There are four types of all-metal PDM lines: short-amplitude internal cycloid, short-amplitude external cycloid, internal and external cycloid normal lines, etc. (Bani Mustafa et al., 2021; Isaev et al., 2022). The more mature line type commonly used in PDM is the general short-amplitude internal oscillating line type. This paper has the short-amplitude internal oscillating line as the research line type.

2.1.1. The motor of line fitting

In the actual machining of all-metal PDM, the equation of the motor's profile cannot be directly machined into shape, but is fitted and machined by discrete point coordinates to form the motor's spiral body (Othman et al., 2004). The least squares method is an important method for curve fitting of motor curve data points. Let the data points on the end face profile of the PDM be (x_t, y_t), and the fitted data points of the cycloidal motor are calculated by polynomial to obtain the multivariate function of the minimum value, as shown in Eq. (2).

$$I = \sum_{t=0}^{n} \left[f_j(x_t) - y_t \right]^2 \tag{2}$$

From the definition of minimum, it follows that the precondition for the existence of a minimum is that the derivative of Eq. (2) is zero, as shown in Eq. (3).

$$\begin{cases} f_j(x_t) = \sum_{j=0}^{p} a_j x_t^j \\ \dfrac{\partial I}{\partial a_k} = 2 \sum_{t=0}^{q} \left(\sum_{j=0}^{p} a_j x_t^j - y_t \right) x_t^k \end{cases} \tag{3}$$

The a_k in this formula can be derived from Eq. (3), which leads to

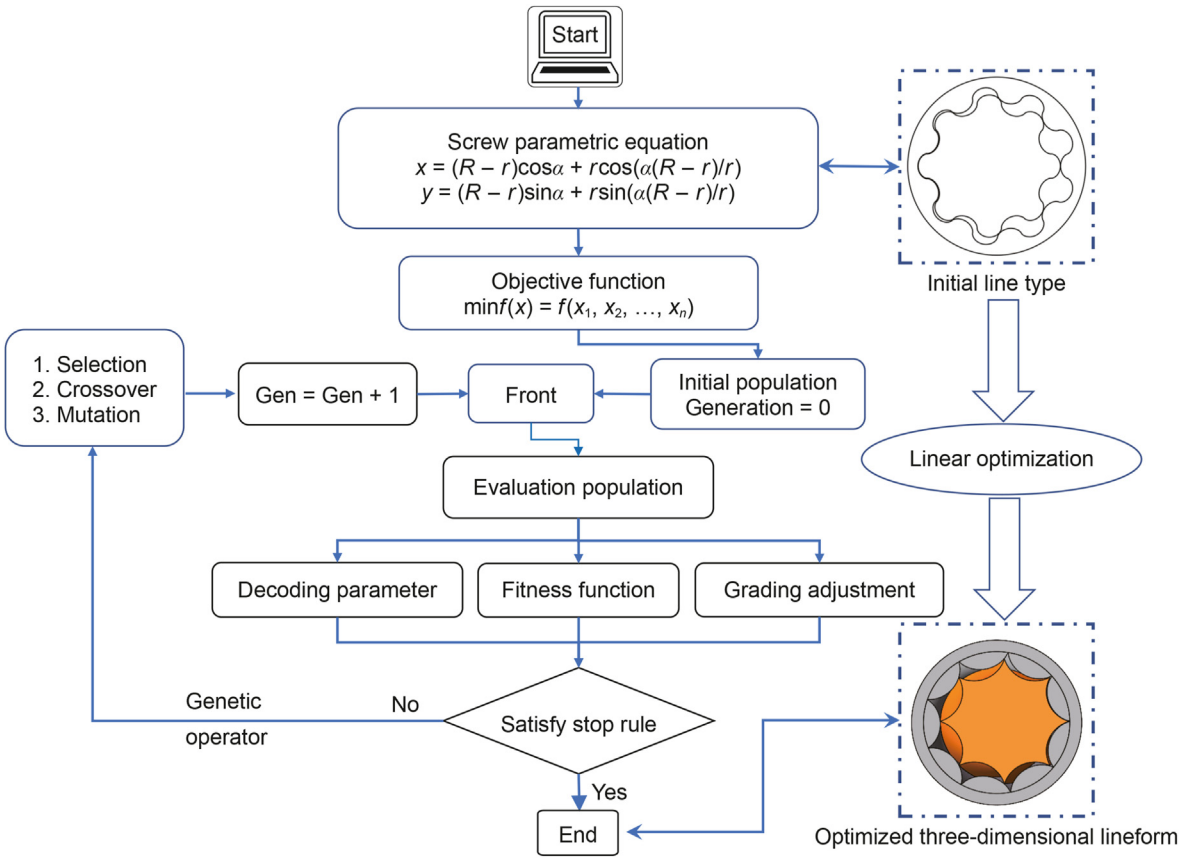

Fig. 1. The flow chart of motor line optimization.

the fitting function, as shown in Eq. (4).

$$\begin{cases} a_0+a_1\sum_{j=0}^{p}x_j+a_2\sum_{j=0}^{p}x_j^2+\bullet\bullet\bullet+a_n\sum_{j=0}^{p}x_j^n=\sum_{j=0}^{p}y_j \\ a_0\sum_{j=0}^{p}x_j+a_1\sum_{j=0}^{p}x_j^2+a_2\sum_{j=0}^{p}x_j^3+\bullet\bullet\bullet+a_n\sum_{j=0}^{p}x_j^n=\sum_{j=0}^{p}x_jy_j \\ \cdots \\ a_0\sum_{j=0}^{p}x_j^n+a_1\sum_{j=0}^{p}x_j^{n+1}+a_2\sum_{j=0}^{p}x_j^{n+2}+\bullet\bullet\bullet+a_n\sum_{j=0}^{p}x_j^{2n}=\sum_{j=0}^{p}x_j^ny_j \end{cases} \tag{4}$$

Among them, $k\in N^+$, $j\in N^+$, $p\in N^+$.

In the linear fitting of the PDM, a multivariate system of equations is required to calculate the linear equations. The common method is the Gaussian fitting method, firstly, by transforming the coefficient matrix of the cycloidal motor equations into a triangular matrix. Secondly, the solution of the system of equations is obtained by back substitution one by one, which is the linear solution of the PDM. Finally, the matrix transformation is performed by transforming the row with the largest absolute value through the row transformation matrix, which makes the matrix algorithm more accurate.

2.1.2. Spline curve fitting

In this section, polynomial interpolation is introduced to solve the PDM line fit. The integrated interpolation condition, continuity condition, and boundary condition are used to calculate the spline interpolation function of the PDM, which is obtained by the PDM line continuity condition as well as the boundary condition, as shown in Eq. (5).

$$\begin{bmatrix} 2 & \lambda_1 & & & \\ a_2 & 2 & \lambda_2 & & \\ \ddots & \ddots & \ddots & & \\ & \ddots & \ddots & \ddots & \\ & & a_{n-2} & 2 & \lambda_{n-2} \\ & & & a_{n-1} & 2 \end{bmatrix} \begin{bmatrix} x_1 \\ x_2 \\ \vdots \\ \vdots \\ x_{n-2} \\ x_{n-1} \end{bmatrix} = \begin{bmatrix} c_1-a_2x_0 \\ c_2 \\ \vdots \\ \vdots \\ c_{n-2} \\ c_{n-1}-\lambda_{n-1}x_n \end{bmatrix} \tag{5}$$

Eq. (6) can be obtained by calculation Eq. (5).

$$\begin{cases} a_kx_{k-1}+2x_k+\lambda_kx_{k+1}=c_k \\ 1\ll k\le n-1 \\ \lambda_k=1-a_k \\ c_k=6f[x_{k-1},x_k,x_{k+1}] \end{cases} \tag{6}$$

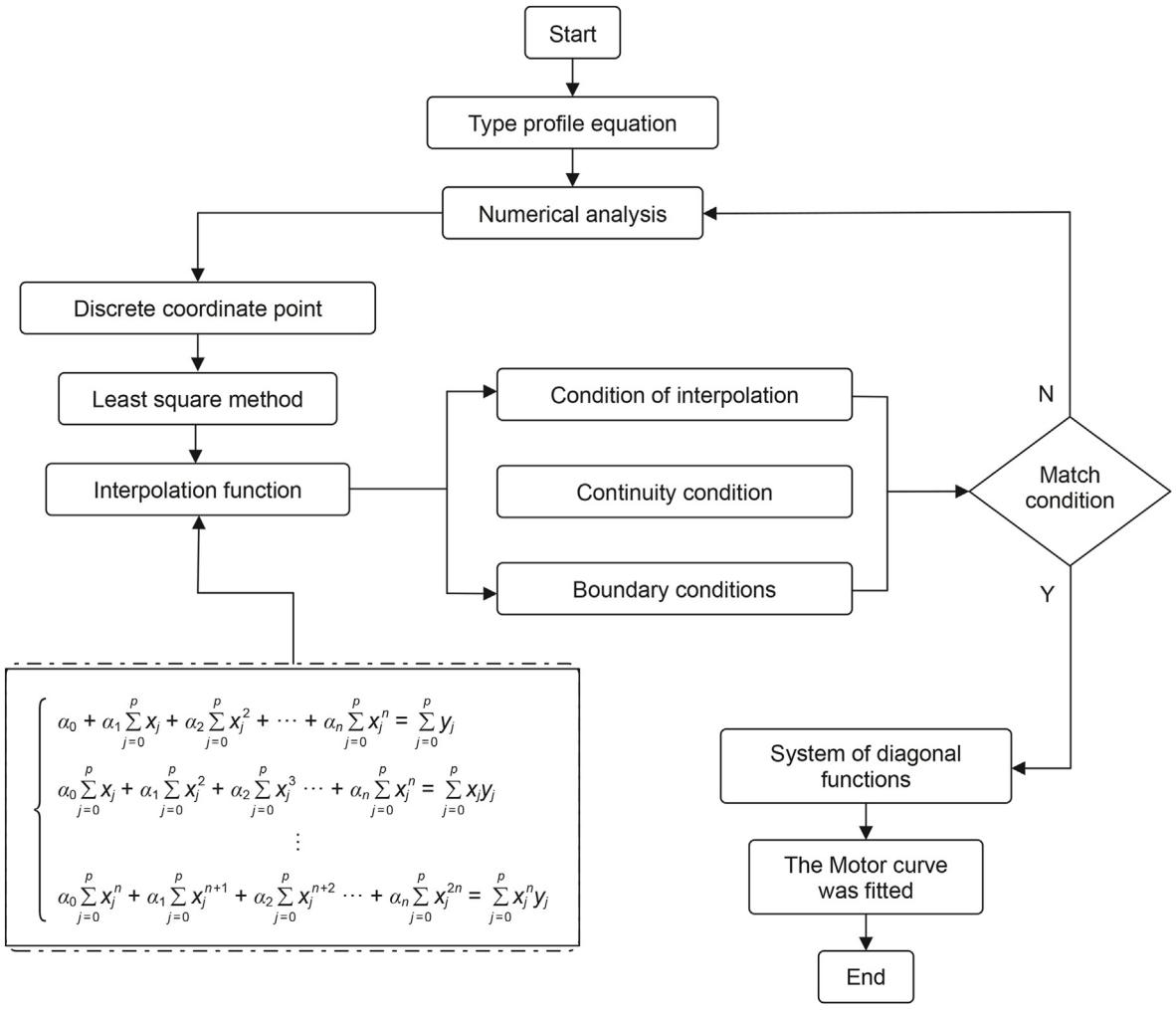

Fig. 2. The curve fitting program diagram.

From Eq. (5) and Eq. (6), it can be seen that the diagonal linear equation system is a strictly diagonal matrix, and by calculating the unique solution of the solvable equation system. The segmental expression of the cubic spline function of the PDM can also be found, and the specific process is shown in Fig. 2.

As can be seen from Fig. 2, the curve fitting of PDM motor is generated by multiple fitting of the basic fitting function. Through the above content, it is necessary to establish the initial parameters of the motor for the data discretization fitting curve. The initial parameters of the end face profile of the PDM are shown in Table 1.

The PDM obtains discrete data points by interpolating the spline function and setting the boundary conditions, and the data points are not continuously smooth. To realize the fitting from discrete data points to a smooth curve, the more the number of fitting nodes, the interpolation function gradually tends to be overlapped by the interpolation function, as shown in Fig. 3.

As can be seen from Fig. 3, during the curve fitting process, the angle of the rotor was adjusted. Fig. 3(a) is the motor curve discrete data points. The orange data points are discrete points on the rotor curve. The blue data points are the discrete points of the stator curve. Fig. 3(b) is the motor fit curve. The orange curve is the rotor fitted line shape. The blue curve is the stator fitting line shape.

2.2. Calculation of linear parameters

2.2.1. Motor curvature and eccentricity calculation

In the process of PDM line design, the cycloid equation is used to derive the motor section bone line equation. The motor section curve is drawn from the bone line equation. Then, the contour of motor section is drawn by equidistance method. The curvature and

Table 1
Initial parameter setting of the motor.

Parameter	Name				
	Number of rotor heads	Number of stator heads	Equidistant radius factor	Eccentricity	Cross-flow area
Symbols	N	N+1	r^0	e	$A(x)$
Unit				mm	mm^2
Initial values	8	9	6.78	6.5	–

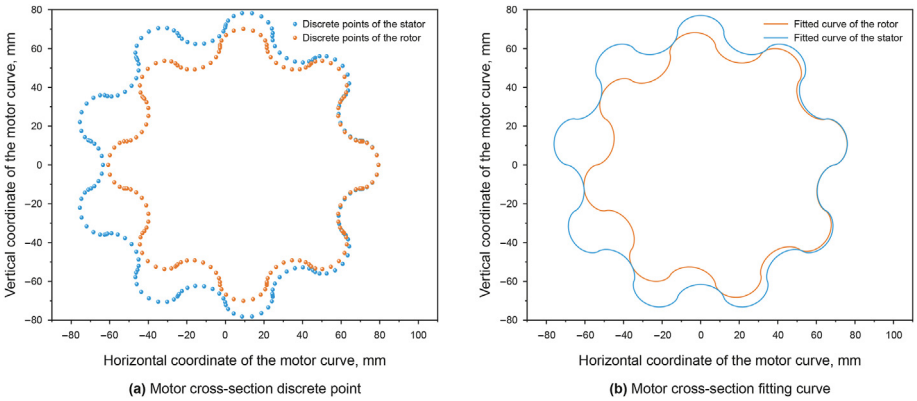

Fig. 3. The curve fitting comparison of PDM.

eccentricity of PDM are calculated based on the theory of PDM short hypocycloid, as shown in the Eq. (7).

$$\begin{cases} E = \dfrac{2R_s}{2(N+1+r^0)} \\ K = \dfrac{N-2}{4(n-1)\left|\sin\dfrac{N\theta}{2}\right|} \end{cases} \tag{7}$$

2.2.2. Contact force calculation

During the operation of a PDM, the stator and rotor interact with each other at all times, touching and rubbing against each other. So, it is crucial to analyze the forces on the rotor during the operation of the PDM. Firstly, the rotor in the motor is subjected to the axial fluid pressure of the drilling fluid, which decreases gradually along the spiral body. Secondly, the rotor is subjected to radial forces on the stator surface, with the direction of the forces perpendicular to the inner helix surface of the stator. Finally, the rotor is subjected to frictional forces due to slip as it rotates in conjunction with the stator, as well as frictional forces on the rotor due to solid particles in the drilling fluid. The viscosity of the drilling fluid and the content of solid particles are critical to the influence of the friction coefficient between the motor rotor and the stator. By analyzing the cross-sectional forces of the PDM, the relationship was obtained, as shown in Fig. 4.

As can be seen from Fig. 4, let the centers of curvature circles of the stator and rotor of the all-metal PDM be O_1 and O_2, respectively, tangent to each other at point P, with radii R_1 and R_2, respectively, and tangent auxiliary surface at tangent point P. Since the local details of point P are not clear, point P is partially intercepted and enlarged by 3 times. Meanwhile, point P is the origin of the coordinate system $X'O'Y'$, the point on the stator is A_1, the corresponding point on the rotor is A_2, and the distances to the auxiliary line are L_1 and L_2, respectively. The rotor and stator contact point P act on each other, so let the rotor act on the stator force is F, and the direction is the same as the normal line of point P, as shown in Eq. (8).

$$\begin{cases} x = (R-r)\cos\alpha + r\cos\left(\dfrac{R-r}{r}\alpha\right) \\ y = (R-r)\sin\alpha - r\sin\left(\dfrac{R-r}{r}\alpha\right) \end{cases} \tag{8}$$

According to the force relationship between the stator and the

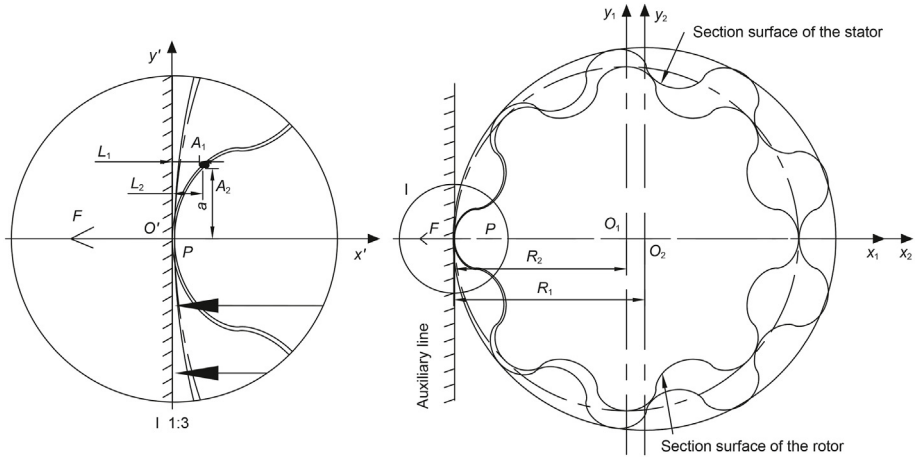

Fig. 4. Motor cross-sectional force diagram.

rotor of the PDM, the contact pressure per unit length of the rotor and the stator contact point P can be expressed, as shown in Eq. (9).

$$F_p = \frac{E\sigma\pi}{(3-4\mu)(1+\mu)+2(1-\mu)\ln\frac{(L_2-L_1)R_1R_2}{2(R_1-R_2)}} \tag{9}$$

where E is the stator elastic modulus of PDM. σ is the Poisson's ratio of the stator.

2.2.3. Computational dynamics model

The displacement volume of an all-metal PDM is defined as the volume of drilling fluid discharged during one cycle of motor operation. The volume chamber in which the stator and rotor of the motor engage varies with the rotation of the motor operation. Assuming that the number of motor stator teeth is N, then the chamber also undergoes N changes during one week of motor operation, forming a cycle. Therefore, it is only necessary to calculate the cross-sectional area of the first chamber in one cycle to calculate the entire cross-sectional area, and then the motor displacement can be calculated, as shown in Fig. 5.

As can be seen from Fig. 5, this section establishes a coordinate system $x_1O_1y_1$ with the center of the motor rotor as the origin O_1, and a coordinate system $x_2O_2y_2$ with the center of the stator as O_2. The radius of the tooth top circle of the stator is R_s, and the radius of the tooth root circle is R'_s. The radius of the tooth top circle of the rotor is R_t and the radius of the tooth root circle is R'_t. The stator and rotor meshing points A1–A9, where A1–A2 are adjacent meshing points and B1–B2 are adjacent points of the stator tooth arc, then the area formed by $\widehat{A_1A_2}$. The $\widehat{A_1B_1}$ and $\widehat{B_1B_2}$ and $\widehat{B_2A_2}$ are sealed rooms. From the polar surface area equation and the transformed direct coordinate relationship, it is obtained in Eq. (10).

$$\begin{cases} S = \dfrac{\int \rho^2(\theta)\mathrm{d}\theta}{2} \\ \rho^2(\theta) = x^2(t) + y^2(t) \\ \theta(t) = \arctan\dfrac{y(t)}{x(t)} + c \end{cases} \tag{10}$$

where S is the area of the adjacent teeth of the stator and rotor of the motor.

When calculating the overflow area of the motor, it is only necessary to calculate the area of the inner curve of the stator and the area of the rotor cross-section respectively, and the difference between them is the overflow area of the motor. As can be seen from Fig. 5, the area formed by the circle of the stator tooth root and tooth top of the motor S_1 and S_2 are equal. The area of the stator internal curve is centered on the intersection point of the stator tooth tip and the tooth root curve. The same applies to the calculation of the cross-sectional area of the rotor. The area formed by the tooth top circle and tooth root circle of the rotor. The S_3, and S_4 are equal, then we get the Eq. (11).

$$\begin{cases} R_s = \left(N+r^0\right)R \\ R_t = \left(N+1+r^0\right)R \\ S_s = \left[N\left(N\pi-\pi+8r^0\right)+\pi\left(r^0\right)^2\right]R^2 \\ S_t = \left[(N-1)\left(N\pi-2\pi+8r^0\right)+\pi\left(r^0\right)^2\right]R^2 \end{cases} \tag{11}$$

where S_s is the stator inner curve area. S_t is the rotor cross-sectional area. R_s is the stator outer circle radius. R_t is the rotor outer circle radius. R is the roll circle radius.

According to the displacement formula of the PDM and the flow area, it can be obtained as shown in Eq. (12).

$$\begin{cases} A_s = \dfrac{\left[2(N-1)\pi+8r^0\right]D^2}{4\left(N+1+r^0\right)^2} \\ q = NT_s(S_s-S_t) \end{cases} \tag{12}$$

where A_s is the motor overflow area. q is the volume excluded by one rotation of the motor. N is the number of motor rotor heads. T_s is the motor stator lead. D is the stator outer profile diameter.

The performance output model of PDM is introduced through the displacement equation and the flow area of the motor, as shown in Eq. (13).

$$\begin{cases} n_t = \dfrac{20Q}{3T_s(S_s-S_t)} \\ M = \dfrac{N\Delta PT_s(S_s-S_t)}{2\pi} \end{cases} \tag{13}$$

where n_t is the motor rotation speed. Q is the motor flow rate. ω is the angular speed of the motor. M is the motor torque. ΔP is the motor pressure drop. N is the number of motor stator heads. T_s is the motor lead.

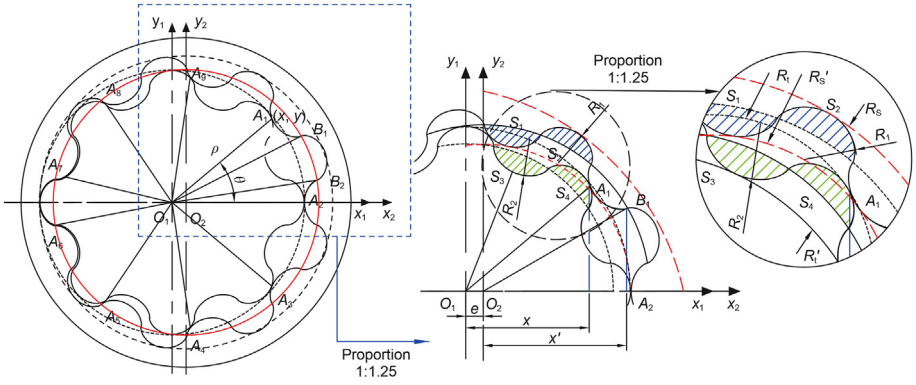

Fig. 5. Overflow area calculation schematic.

2.2.4. Evaluation of motor friction

Due to the complex surface combination of the stator and rotor, the friction calculation is complicated and may not be accurate. According to the working principle of PDM, the greater the relative slip speed of the stator and rotor, the higher the friction coefficient of the motor, while the wear of the stator and rotor of the motor is decreasing. So, the relative slip speed of the stator and rotor of the motor is used to assess the influence of the stator and rotor friction on the service life of the motor. The force and slip of the motor are shown in Fig. 6.

As can be seen from Fig. 6, the all-metal PDM with an 8-head rotor designed in this paper has 8 cusps on the rotor bone line. The relative slip velocity between the stator and rotor can be calculated by the instantaneous center method. Then, the relative slip velocity at the contact point is the product of the distance from the velocity instantaneous center to the contact point. Therefore, the wear rate of stator and rotor of motor is established and the performance loss of motor is evaluated. The B-slip velocity expression of the contact point between rotor and stator teeth of cycloidal motor is obtained, as shown in Eq. (14).

$$\begin{cases} V_x = (-Ne\sin 2t + R_t\cos t)\omega \\ V_y = (Ne\cos 2t + R_t\sin t)\omega \end{cases} \tag{14}$$

where ω is the angular speed of motor rotation.

At the same time, combined with Fig. 6, it can be seen that the geometric relationship between the motor stator profile radius and the rotor profile radius, as shown in Eq. (15).

$$\omega = \frac{2\pi Q}{9T_s(S_s - S_t)} \tag{15}$$

where T_S is the leader of the stator.

Therefore, the slip velocity at point B is obtained, as shown in Eq. (16).

$$\begin{cases} V = w\sqrt{R_t^2 + (Ne)^2 - 2eNR_t\sin t} \\ V_{max} = \dfrac{[(N+r^0)r + Ne]\pi n}{30} \end{cases} \tag{16}$$

where V indicates the motor sliding speed. n is the speed of the motor. V_{max} vindicates the maximum slip speed of the motor.

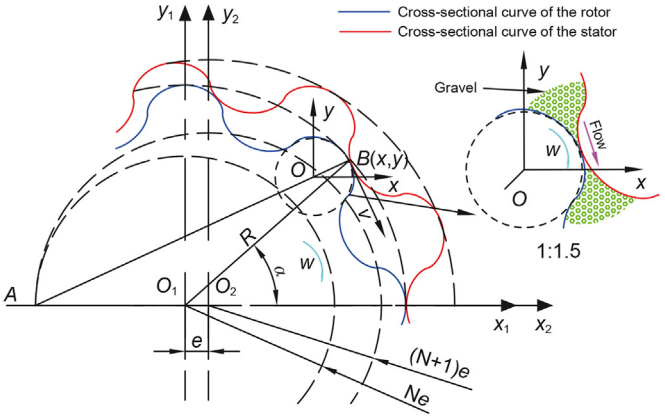

Fig. 6. Contact point slip diagram of PDM.

3. Motor parameter optimization

3.1. Variable setting

The parameter optimization of all-metal PDM focuses on the maximum output torque of the motor. Firstly, it is to improve the motor flow area, that is, the parameter optimization of the motor cross-section area, which is equivalent to improving the motor torque optimization. Secondly, the sliding speed of the PDM is another important indicator affecting the performance of the motor output, mainly because the sliding speed affects the friction between the motor stator and rotor. The greater the relative sliding speed of the two contact points. The stator and rotor wear of the motor are relatively reduced. The service life of the motor is extended.

Therefore, the performance optimization of the motor boils down to the optimization of the motor torque and relative slip speed, setting the motor overflow area parameter as A_s. The maximum slip speed is optimized for the minimum value of $V_{max}(x)$. The smaller $V_{max}(x)$ is beneficial to reduce motor wear and optimize motor performance.

3.2. Objective function optimization

In this section, the profile parameters that affect the output characteristics of all-metal PDM are optimized. Firstly, the motor's equidistant radius coefficient r^0 is optimized. According to the theory of ordinary cycloid equidistant line, the eccentricity is equal to the radius of a circle. The equidistant radius coefficient $r^0 = x_1$, the eccentricity distance $e = x_2$, and the number of rotor heads of the motor $N = x_3$ are set.

Firstly, the flow area of the PDM affects the displacement of the motor and then affects the torque output of the PDM. Because the genetic algorithm optimizes the minimum value, the minimum value of A_s is calculated by optimizing the negative value of A_s, that is, the maximum value of A_s.

Then, the flow area A_s of the first objective function is assumed to be $A_s = f_1(x_1,x_2,x_3)$. Secondly, the relative slip speed of the stator and rotor is another important parameter affecting motor performance output, so the motor slip speed is optimized, and the second objective function $V_{max} = f_2(x_1,x_2,x_3)$ is set. At the same time, the eccentricity of the PDM affects the centrifugal inertia force of the motor rotor and the force on the card and shaft. The smaller the eccentricity is, the better, so the third objective function of the motor $E = f_3(x_1,x_2,x_3)$ is set, as shown in Eq. (17).

$$\begin{cases} \min f_1(x_1,x_2,x_3) = -\dfrac{[2(x_3-1)\pi + 8x_1]D^2}{4(x_3+1+x_1)^2} \\ \min f_2(x_1,x_2,x_3) = \dfrac{2(x_3+1+x_1)^2(2x_3x_2 + x_1x_2)Q\pi}{15(x_3+1)x_3h[2(N-1)\pi + 8x_1]D^2} \\ \min f_3(x_1,x_2,x_3) = \dfrac{R_s}{x_3+1+x_1} \end{cases} \tag{17}$$

3.3. Constraint condition

According to the cycloid principle and empirical formula of PDM, the range of equal radius coefficients and head numbers can be summarized from the Baker Hughes handbook. The value range of eccentricity can be obtained from the researches of Nguyen et al.

(2018) and Baker Hughes (2020), as shown in Eq. (18).

$$\text{s.t.}\begin{cases} 0<x_1<8 \\ 0<x_2<12 \\ 0<x_3<9 \end{cases} \tag{18}$$

3.4. Optimization and linear generation

The mathematical model for optimization of PDM linear parameters developed in Sections 3.2 and 3.3 was used to optimize the cross-flow area that affects the screw performance output. In the optimization of the PDM genetic algorithm, the variation rate is taken as 0.02 and the crossover rate is taken as 0.15. Because the variation rate is too small to easily lose the diversity of the population and the variation rate is too large to destroy the favorable population fraction. Secondly, the population is taken as 60 and the maximum number of iterations is 80. So, Eq. (19) is obtained.

$$\begin{cases} \min f_1(x_1,x_2,x_3) = -\dfrac{[2(x_3-1)\pi+8x_1]D^2}{4(x_3+1+x_1)^2} \\ D = 156\ \text{mm} \\ Pop = 80 \\ pm = 0.01 \\ pc = 0.6 \\ gen = 80 \end{cases} \tag{19}$$

where *Pop* denotes population size. *pc* denotes crossover. *pm* denotes mutation. *gen* denotes the number of iterations.

By substituting known parameters into Eq. (20), the objective function of motor objective optimization is obtained, as shown in Eq. (20).

$$\text{Objective}\begin{cases} \min f_{N=9}(X,Y) = -\dfrac{60.84\times[6.28(Y-1)+8X]}{(1+X+Y)^2}\ (9\ll Y\le 10) \\ \min f_{N=8}(X,Y) = -\dfrac{60.84\times[6.28(Y-1)+8X]}{(1+X+Y)^2}\ (8\ll Y\le 9\ ) \\ \vdots\vdots \\ \min f_{N=3}(X,Y) = -\dfrac{60.84\times[6.28(Y-1)+8X]}{(1+X+Y)^2}\ (3\ll Y\le 4) \end{cases} \tag{20}$$

The genetic algorithm is used to optimize the parameters of the PDM. The general steps are as follows: (1) It is preferred to determine how to code each parameter according to the design parameters of the screw, such as binary coding, integer coding, etc. (2) Initialize the population: randomly generate some individuals as the initial population. (3) Calculate the fitness function: decode the genes of each individual into actual parameters, and run the simulation model to calculate the screw performance indicators, such as efficiency, torque, etc. These indicators can be used as the value of fitness function to evaluate the quality of an individual. (4) Selection operation: select individuals according to the fitness function, retain individuals with high fitness, and eliminate individuals with poor fitness. (5) Cross operation: the individuals with high fitness are crossed to produce new offspring individuals. (6) Mutation operation: carry out certain probability mutation operation on individual offspring to increase the diversity of the population. Repeat steps 3 through 6 until stopping conditions are met, such as the maximum number of iterations or fitness is high enough. (7) Output optimal solution: the individual with the highest fitness is selected from the final population, which is the optimal parameter of the screw. By importing the objective function programming into Matlab software, the optimal solution process of program operation is shown in Fig. 7.

As can be seen from Fig. 7, the curve change is directly generated by programming and optimizing the objective function in Matlab software. The principle of optimization is to calculate the objective function through many iterations, so that multiple objective functions can get the best value. When the optimized curve becomes a straight line, the best results are obtained, and multiple iterative calculations ensure the accuracy of the results. The horizontal coordinate of the curve is the number of iterations. The vertical coordinate is the change of the optimal solution.

Because the calculation result of genetic algorithm fluctuates every time, the fluctuation error is very small. By combining the mathematical model in Section 2, genetic algorithm optimization was carried out several times in matlab software, and the average value of the optimal solution was obtained. The calculated results are shown in Table 2.

It can be seen from Table 2 that when the number of motor heads is 8, the eccentricity is 8.66 mm, the theoretical torque is a maximum of 14176 N·m. Therefore, the profile parameters of PDM are optimized using genetic algorithm for better performance. The profile parameters of the motor stator and rotor are obtained, and the PDM curves are compared before and after optimization in Matlab software, as shown in Fig. 8.

As can been seen from Fig. 8, the curve before the optimization is smooth, and the convex angles of the optimized motor profile are sharp. Because the optimized line is an involute, there is no buckle phenomenon, so the sharp angles of the profile can be smoothly rotated.

By using the motor end profile obtained in Matlab to generate the recognizable curve in CAD software, the stator and rotor curves are imported into Solidworks. The 3D model of the motor before and after optimization was established, and the optimized 3D model was compared with the motor profile experimentally tested by Top Oil Tech Limited of Canada (InFocus Energy Services Inc., 2020). The feasibility of the existence of an involute motor profile

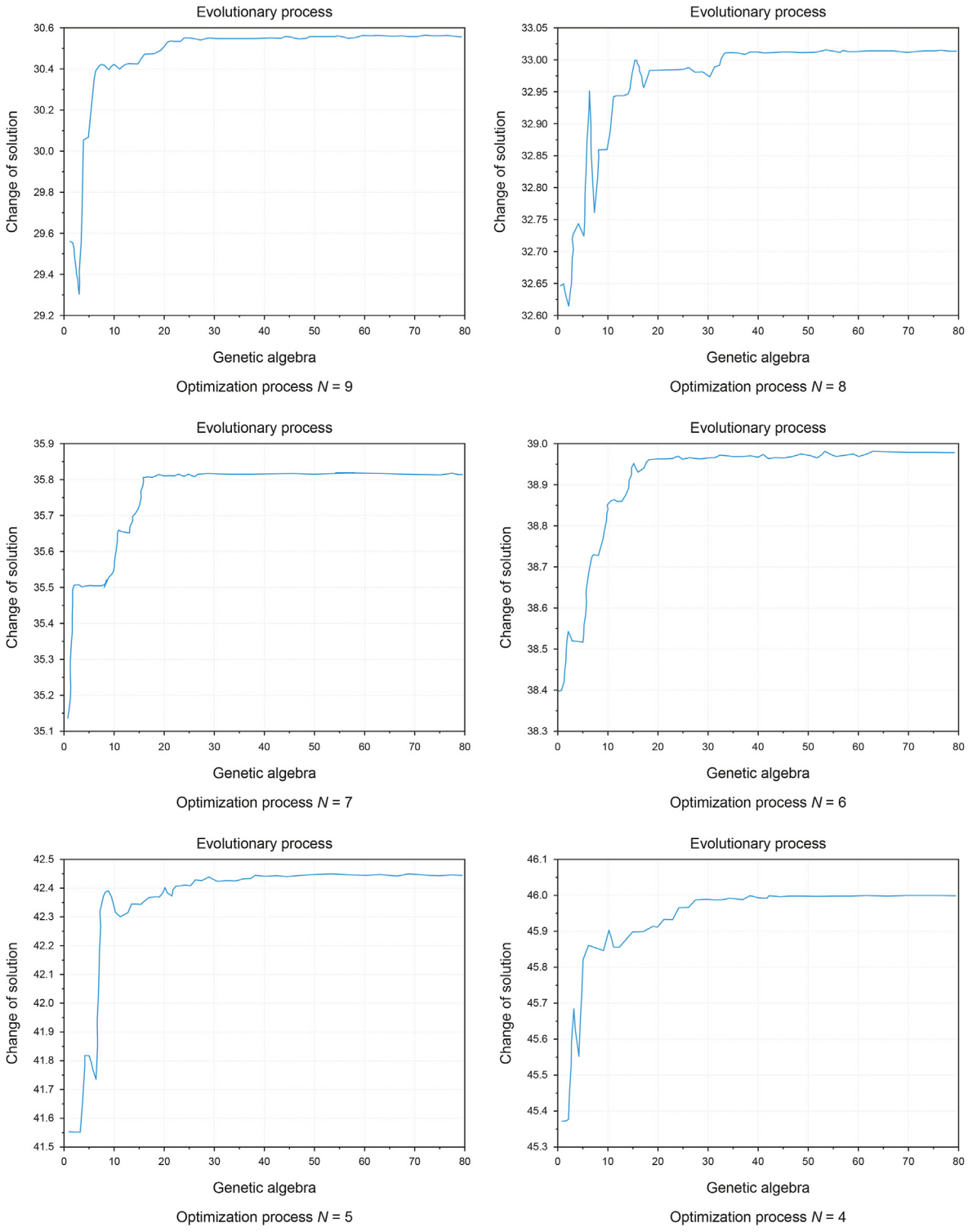

Fig. 7. The process of optimizing program solutions.

with a very small isometric radius is verified, and its three dimensions are shown in Fig. 9.

As can been seen from Fig. 9, the conventional PDM motor is optimized by genetic algorithm. The optimized linear results are consistent with those obtained by InFocus, which proves the feasibility of the optimization method.

4. Parameter optimization analysis

4.1. Influence of flow area on motor

The equidistance radius factor is an important parameter that affects the overflow area of all-metal PDM. Based on the motor overflow area (Eq. (18)), it can be seen that the parameters that

Table 2
Optimize motor r^0 and E parameter results.

Parameters	N						
	8 (Raw data)	8	7	6	5	4	3
Equidistant radius coefficient (r^0)	2.5	0.0019	0.0035	0.0041	0.006	0.29	0.86
Eccentric distance (E, cm)	0.678	0.8664	0.97	1.11	1.3	1.47	1.6
Flow area (A_s, cm^2)	30.88	33.016	35.81	38.98	42.44	46	50.07
Displacement (q, L)	23.8	25.44	21.46	17.5	13.63	9.85	6.4
Maximum slip velocity (V, m/s)	55.03	49.76	54.62	61.39	71.55	87.82	114.4
Rotating speed (n, rpm)	34.04	31.8	37.7	46.2	59.4	85.27	125.98
Torque (N·m)	12633	14176	11960.7	9764.4	7594.3	5487.4	3583.4

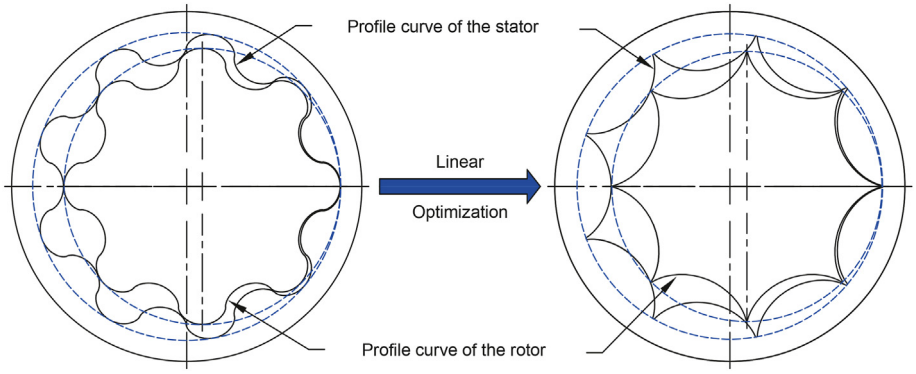

Fig. 8. Comparison of motor profile before and after optimization.

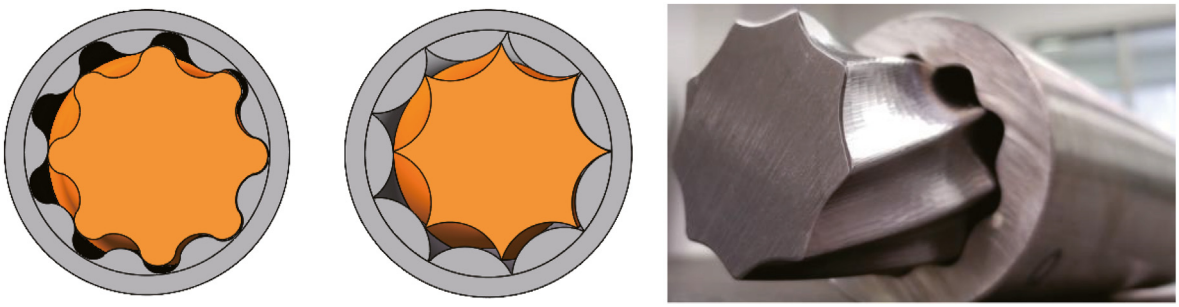

(a) Original line type **(b)** Optimized line shape **(c)** Line shape tested in Canada (InFocus Energy Services Inc, 2020)

Fig. 9. Comparison of line optimization.

affect the motor overflow area are the number of heads of the motor rotor and the equidistance radius factor of the motor profile. By programming the equation of overflow area in Matlab, the variation of motor overflow area with different numbers of heads and equidistant radius coefficient of motor coupling is shown in Fig. 10.

As shown in the Fig. 10, under the working condition of motor, the inlet and outlet pressure is 5 MPa and motor flow rate is 15 L/s. The overflow area of the motor decreases with the increase of isometric radius factor. The displacement of the motor also decreases gradually. The volumetric efficiency of the motor is proportional to the displacement of motor, that is, the volumetric efficiency of the motor decreases gradually. At the same time, the motor overflow area decreases with the number of motorheads, and the motor torque decreases with the increase of the isometric radius factor.

4.2. Slip speed effect on motor

The maximum slip speed of an all-metal PDM affects the wear of motor's stator and rotor. The factors that affect the motor slip speed are the eccentricity and equidistance radius coefficient of the motor. The relationship between the motor eccentricity and equidistance radius coefficient can be expressed numerically based on the objective function Eq. (18). The coupling relationship between the equidistance radius coefficient and eccentricity of the motor is shown in Fig. 11.

As shown in Fig. 11(a), under the condition that the inlet and outlet pressure of the motor is 5 MPa and the flow rate of the motor is 15 L/s, when the number of motors is constant, the eccentricity of the motor decreases with the increase of the isometric radius coefficient of the motor. When the radius coefficient of contour equidistance is constant, the motor eccentricity increases with the

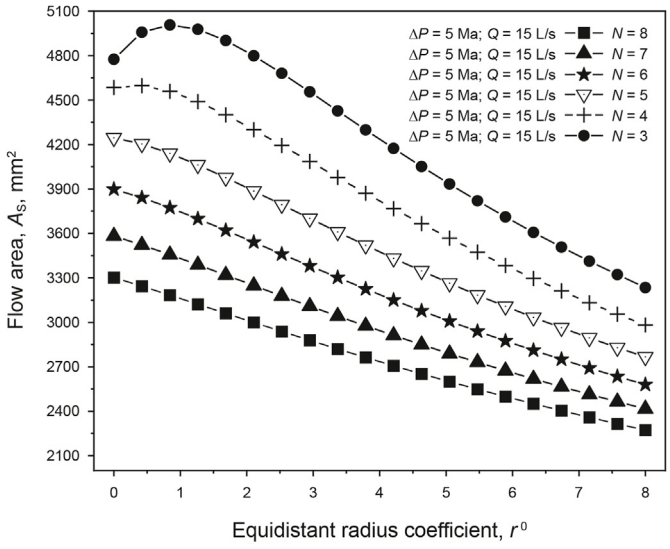

Fig. 10. The influence of r^0 and N about the flow area.

number of rotor heads. As shown in Fig. 11(b), when the motor eccentricity is fixed, the maximum slip velocity of the motor increases with the increase of the motor isometric radius. The maximum slip velocity of the motor increases with the increase of the motor's eccentricity when the motor's constant radius coefficient is fixed.

4.3. Influence of equidistant radius coefficient on motor

The equal radius coefficient of the motor affects the bone line of the motor to generate the end-face line and then affects the displacement of the motor. Based on the numerical calculation of Eq. (18), the isometric radius coefficient, eccentricity, and torque coupling relationship diagram of the motor are programmed in Matlab software, as shown in Fig. 12.

As shown in Fig. 12(a), under the condition that the inlet and outlet pressure of the motor is 5 MPa and the motor flow rate is 15 L/s, when the number of rotor heads of the motor is constant, the torque of the motor decreases with the increase of the isometric radius coefficient. When the radius coefficient is constant, the torque of the motor increases with the number of motors. As shown

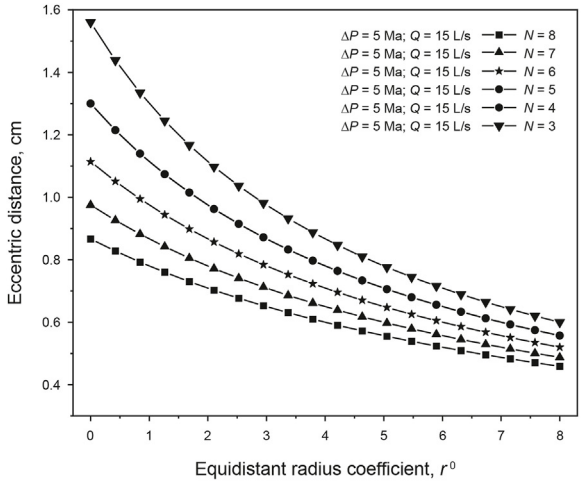

(a) The relationship between r^0 and E

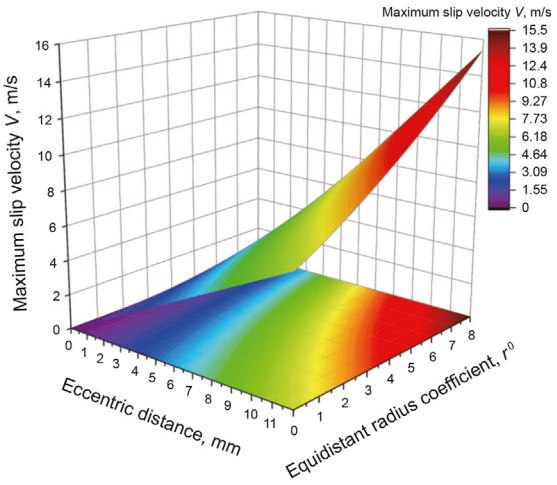

(b) The effect of r^0 and E on slip speed

Fig. 11. The coupling relationship between r^0 and E on slip velocity.

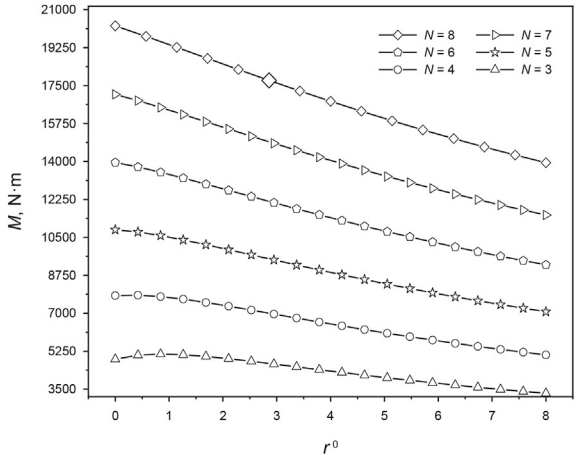

(a) Relationship between r^0 and M

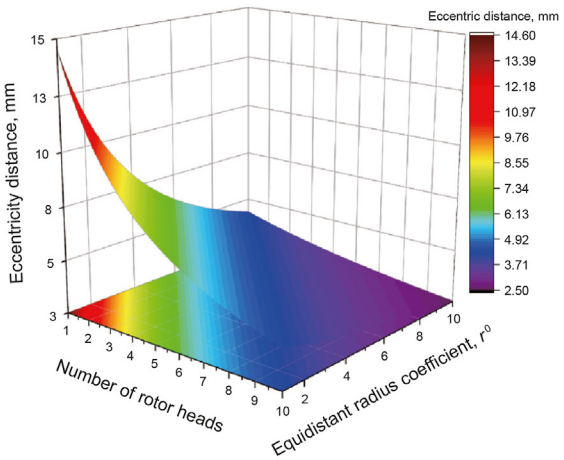

(b) Influence of N and r^0 on the eccentricity

Fig. 12. Influence of equidistant radius coefficient on motor.

in Fig. 12(b), when the motor isometric radius coefficient is constant, the motor's eccentricity decreases with the increase in the number of motors, and the trend increases first and then decreases. When the number of motorheads is constant, the eccentricity of the motor decreases with the increase of the equidistant radius coefficient.

4.4. Output characteristic analysis

All-metal PDM performance affects the drilling efficiency, on the motor performance analysis based on Section 3.4 optimization parameters and output performance. Introducing InFocus company in 2022, all-metal PDM test 7″ 7|8 Lobe 2.4 Stage experimental data, and evaluate the ascension of the motor performance before and after optimization (InFocus Energy Services Inc., 2018). The calculation of Eq. (21) is as follows.

$$\begin{cases} A_s';\ \eta_n;\eta_n' = \dfrac{n_p - n_q}{n_q} \times 100\% \\ \eta_w;\eta_w' = \dfrac{w_q - w_p}{w_p} \times 100\% \end{cases} \tag{21}$$

where A_s' represents the percentage increase in the flow area before and after motor optimization. η_n represents the percentage increase in motor speed before and after optimization. η_n' indicates the percentage increase in motor speed after optimization relative to InFocus. η_w represents the percentage increase of motor torque before and after optimization. η_w' indicates the percentage increase of motor torque after optimization relative to InFocus. n_p represents the motor speed after optimization. n_q represents the speed before motor optimization. w_p represents torque before motor optimization. w_q represents the optimized torque of the motor.

When optimizing the parameters of the PDM, the outside diameter size was selected to be the same as that of the InFocus. The parameters of the optimal solution are obtained step by step, and the optimization results are obtained through modeling and numerical analysis. This optimization process is slightly different from the parameters tested experimentally by InFocus, but the comparison results are within a reasonable margin of error. The comparison results are shown in Table 3.

As shown in Table 3, the overflow area of the optimized motor is increased by 6.9%. The motor speed calculated by the profile parameters before optimization was 34.04 rpm, and the motor profile speed after optimization was 31.8 rpm, which reduced the original speed by 6.58%. The torque of the motor before optimization was 12633 N·m. The torque of the motor after optimization was 14176 N·m, which increased the torque by 12.21%. At the same time, the experimental data of InFocus tested in 2020 was introduced for comparison, and the specific data comparison is shown in Fig. 13.

As can be seen from Fig. 13, the motors tested by the InFocus use 7-head rotors, whose speed is 25 rpm and torque is 10208 N·m.

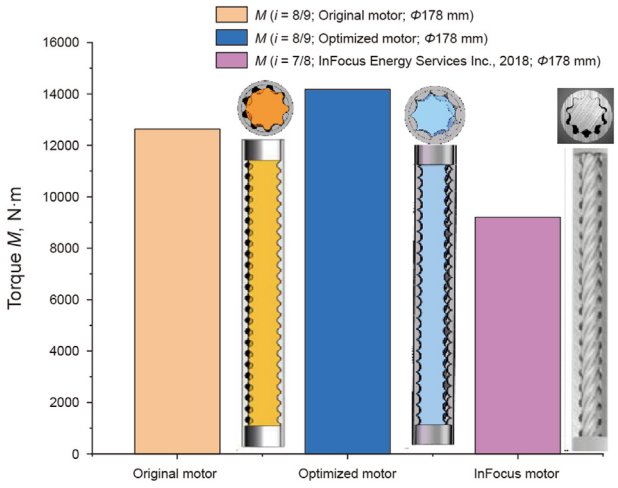

Fig. 13. The torque comparison between optimization and InFocus experiments (InFocus Energy Services Inc., 2018).

After optimization, the motor profile speed is 31.8 rpm and the torque is 14176 N·m, and the speed is increased by 27.2% compared with the motor of InFocus. That's a 38.8% increase in torque over the motors tested by InFocus.

5. Conclusions

In this paper, the least square method was used to design the initial motor profile fitting. The motor dynamic model was numerically calculated with the motor profile parametric equation. The objective function of the all-metal PDM profile optimization was established. Then, the optimized motor profile was obtained and verified with the motor profile tested by Top Oil Tech Limited in Canada. By using a genetic algorithm programmed in Matlab, the motor objective function was optimized. The effects of equidistant radius coefficient and eccentricity coupling on the flow area, maximum slip speed and torque of the motor are obtained. Compared with InFcous experimental test data, the following conclusions are drawn.

(1) Under the same working condition, the flow area of all metal PDM decreases with the increase of equidistance radius coefficient. The volumetric efficiency of the motor also decreases with the increase of the equidistant radius coefficient.
(2) Under the same operating conditions, the relative maximum slip speed of the motor increases with the increase of the radius coefficient of the motor. So that the motor wear more and more serious.
(3) In the structure of the motor, the eccentricity decreases with the increase of the isometric radius coefficient. The more the

Table 3
Motor-optimized front and rear output characteristics.

Indicators	Name		
	Original line type	Optimized line shape	InFocus, Inc.
Working conditions	$\Delta p = 5$ MPa ; $Q = 15$ L/s ;i=8/9		$\Delta p = 1000$ psi $i = 7/8$
Rotational speed, m/s	34.04	31.8	About 25
Torque, N·m	12633	14176	About 10208
A_s'; η_n ; η_n'	–	6.9%; −6.58%; 27.2%	–
η_w ; η_w'	–	12.21%; 38.8%	–

number of rotor heads, the smaller the eccentricity. Thus, the force on the cardan axis of the motor is improved.

(4) Under the same condition, after the genetic algorithm profile optimization, the motor speed is reduced by 6.58% and the torque is increased by 12.21%.

In addition, the numerical calculation and genetic algorithm optimization results of this paper are compared with those of Top Oil Tech Limited and InFocus Canada. It provides theoretical basis for profile optimization of all-metal PDM. Genetic algorithm optimization method is provided to improve the performance of all-metal PDM. It lays a foundation for the manufacture of all-metal PDM.

Finally, the algorithm optimization based on the function constructed by the mathematical theory of the all-metal PDM has the advantage of multi-objective iterative calculation optimization. This provides a theoretical basis for further optimization of PDM performance in the future. However, there are also some shortcomings, failing to consider the impact of friction and wear on the performance output of the PDM. If the objective function of friction and wear can be added for algorithm optimization, the parameters to improve motor performance output will be further obtained.

CRediT authorship contribution statement

Jia-Xing Lu: Writing – original draft, Software, Methodology, Conceptualization. **Ling-Rong Kong:** Supervision, Investigation. **Yu Wang:** Supervision, Funding acquisition, Formal analysis. **Chao Feng:** Investigation. **Yu-Lin Gao:** Investigation.

Declaration of competing interest

The authors declare that they have no known competing financial interests or personal relationships that could have appeared to influence the work reported in this paper.

Acknowledgment

This work is supported by the National Natural Science Foundation of China (No. 42172343). In addition, great thanks to previous researchers for their excellent work, which has greatly helped academic research.

Appendix A. Supplementary data

Supplementary data to this article can be found online at https://doi.org/10.1016/j.petsci.2024.03.022.

References

Baker Hughes, 2020. Navi Drill Motor Handbook. Available: https://www.bakerhughes.com/sites/bakerhughes/files/2020-11/Baker-Hughes-Navi-Drill-motor-handbook-15th-edition-2020.PDF.

Bani Mustafa, A., Abbas, A.K., Alsaba, M., 2021. Improving drilling performance through optimizing controllable drilling parameters. Journal of Petroleum Exploration and Production 11, 1223–1232. https://doi.org/10.1007/s13202-021-01116-2.

Baskal, T., 2014. Optimization of screw elements by genetic algorithm. Mater. Test. 56, 1049–1053. https://doi.org/10.3139/120.110664.

Beauquin, J.L., Boireau, C., Lemay, L., 2005. Development status of a metal progressing cavity pump for heavy oil and hot production wells. OnePetro. https://doi.org/10.2118/0506-0059-JPT.

Cao, G., Zhang, J., Guo, Y., et al., 2022. Numerical modeling on friction and wear behaviors of all-metal progressive cavity pump. J. Petrol. Sci. Eng. 213, 110443. https://doi.org/10.1016/j.petrol.2022.110443.

Chaturvedi, E., Acar, P., Sandu, C., 2023. Multi-objective macrogeometry optimization of gears: comparison between sequential quadratic programing and genetic algorithm. Mech. Base. Des. Struct. Mach. 51, 97–112. https://doi.org/10.1080/15397734.2022.2146710.

El-Abd, F.M., Wahba, E.M., Adam, I.G., 2020. Viscous flow simulations through multi-lobe progressive cavity pumps. Petrol. Sci. 17, 768–780. https://doi.org/10.1007/s12182-020-00458-6.

Gaymard, B., Chanton, E., Puyo, P., 1988. The progressing cavity pump in Europe: results and new developments. In: Offshore South East Asia Show. https://doi.org/10.2118/17676-MS. February 2–5, Singapore.

Guo, C., Tang, Y., 2003. Influence of process parameters on screw rotor profiles. Mach. Sci. Technol. 7, 105–118. https://doi.org/10.1081/MST-120018957.

InFocus Energy Services Inc., 2018. AMP: all metal power sections. Available: https://www.infocusenergy.com/amp-power-sections.

InFocus Energy Services Inc., 2020. Developing downhole oil and gas drilling products faster with structural simulation engineer. Available: https://files.solidworks.com/casestudies_eng/pdf/InFocusEnergy_FINAL_022519.pdf.

Isaev, A.A., Aliev, M.M.O., Drozdov, A.N., et al., 2022. Improving the efficiency of curved wells' operation by means of progressive cavity pumps. Energies 15 (12), 4259. https://doi.org/10.3390/en15124259.

Lea, J., Anderson, P., Anderson, D., 1988. Optimization of progressive cavity pump systems in the development of the clearwater heavy oil reservoir. J. Can. Petrol. Technol. 27 (1). https://doi.org/10.2118/88-01-05. PETSOC-88-01-05.

Lehman, M., 2004. Progressing cavity pumps in oil and gas production. World Pumps 20–22. https://doi.org/10.1016/S0262-1762(04)00356-6.

Li, M., Jiang, D., Guo, H., 2017. Study on clearance optimization of all-metal screw pumps: experiment and simulation. Study on Clearance Optimization of All-metal Screw Pumps Mechanics 23, 735–742. https://doi.org/10.5755/j01.mech.23.5.15387.

Liang, C., Wang, Y., Peng, Z., 2023. Influence of surface roughness of stator on dry sliding behavior against rotor in pneumatic downhole motor. J. Mater. Eng. Perform. 32, 2392–2407. https://doi.org/10.1007/s11665-022-07254-w.

Lu, J., Wang, Y., Kong, L., 2023. Analysis of output performance of all-metal progressive cavity motor. Geoenergy Science and Engineering 222, 211456. https://doi.org/10.1016/j.geoen.2023.211456.

Marius, S., 2018. On the Durability of Progressive Cavities Pumps, vol. 1. Fiabilitate şi Durabilitate. https://www.researchgate.net/publication/325595039_ON_THE_DURABILITY_OF_PROGRESSIVE_CAVITIES_PUMPS.

Nguyen, K., Nguyen, T.C., Al-Safran, E., 2021. Modeling the performance of progressive cavity pump under downhole conditions. J. Petrol. Sci. Eng. 198, 108121. https://doi.org/10.1016/j.petrol.2020.108121.

Nguyen, T., Al-Safran, E., Saasen, A., et al., 2014. Modeling the design and performance of progressing cavity pump using 3-d vector approach. J. Petrol. Sci. Eng. 122, 180–186. https://doi.org/10.1016/j.petrol.2014.07.009.

Nguyen, T.C., Al-Safran, E., Nguyen, V., 2018. Theoretical modeling of positive displacement motors performance. J. Petrol. Sci. Eng. 166, 188–197. https://doi.org/10.1016/j.petrol.2018.03.04.9.

Othman, M., Mohamed, A., Hussain, A., 2004. Fast Evaluation of Available Transfer Capability (Atc) Considering Integral Square Generator Angle (Isga), pp. 253–257. http://www.wseas.us/e-library/transactions/power/2008/25-806N.pdf.

Rong, X., Zhu, H., Hu, B., 2021. Performance research and structure optimization of labyrinth screw pump. Micromachines 12 (7), 790. https://doi.org/10.3390/mi12070790.

Samuel, G.R., Saveth, K.J., 2006. Optimal design of progressing cavity pumps (pcp). Journal of Energy Resources Technology-transactions of the Asme 128, 275–279. https://doi.org/10.4115/1.2358142.

Tschirky, J.E., 1978. New developments in down-hole motors for improved drilling performance. J. Petrol. Technol. 30, 993–997. https://doi.org/10.2118/6778-PA.

Wan, B.L., 1993. Single Screw Hydraulic Machinery. University of Petroleum Press (in Chinese).

Wang, J., Pan, S., Dong, L., et al., 2022. Modelling of a novel progressive cavity pump with a special internal compression process used in oil wells. J. Petrol. Sci. Eng. 217, 110889. https://doi.org/10.1016/j.petrol.2022.110889.

Wang, Y., Yu, X., Han, X., et al., 2021. Influences of eccentricity ratio on the internal flow and cavitation characteristics of progressing cavity pump. Proc. IME C J. Mech. Eng. Sci. 235, 6111–6121. https://doi.org/10.1177/0954406221998401.

Whitley, D., 1994. A genetic algorithm tutorial. Stat. Comput. 4, 65–85. https://link.springer.com/article/10.1007/BF00175354.

Zhang, D., Guo, P., Hu, Q., et al., 2022. Parametric study and multi-objective optimization of a ductless archimedes screw hydrokinetic turbine: experimental and numerical investigation. Energy Convers. Manag. 273, 116423. https://doi.org/10.1016/j.enconman.2022.116423.